Pre-processing and Assessment of Rain Drop Size Distributions Measured with a K-band Doppler Radar and an Optical Disdrometer

José Manuel Riera, *Senior Member, IEEE*, Ana Benarroch, Pedro Garcia-del-Pino and Santiago Pérez-Peña

***Abstract*—Rain attenuation in millimeter-wave links depends on the Drop Size Distributions (DSD) of the raindrops. Empirical models disregard this dependence and estimate the specific attenuation using only the integrated rainfall rate (*R* (mm/h)). This approach is valid for lower frequencies but it progressively losses accuracy as the frequency of interest becomes higher within the millimeter-wave range. Both the characterization of rainfall phenomena and the prediction of rain attenuation can be improved with the knowledge of DSD, which, in turn, depend on the type of rain event (stratiform or convective) and the *R*. In this paper, long-term DSD measurements from a vertical Doppler radar (MRR-2) and a laser optical disdrometer (Thies Laser disdrometer) are used to obtain, classify and compare the statistics of DSD in Madrid in periods of more than ten years. The process to obtain the DSD from these advanced instruments is analyzed in detail, providing recommendations about the calibration of the radar data and the most appropriate particle filtering to apply on the Laser disdrometer data.**

Index Terms— Atmosphere, Radar Data, Optical Data

I. Introduction

MILLIMETER-WAVE communication systems are being increasingly used in the context of the growing demand for high capacity services. Links operating in these frequency bands are subject to propagation effects arising from the interactions of the electromagnetic waves with the atmosphere constituents. Rain attenuation is the most relevant effect, since it causes very deep fades that can compromise the link availability. It is mainly produced by liquid particles, since ice crystal and snowflakes cause much lower attenuation at these frequencies. In lower frequency bands, rain attenuation can be estimated with little error from the rainfall rate (*R* (mm/h)) [1]-[2] that, together with the frequency and polarization, are sufficient to provide an estimation of the specific attenuation suffered by the signal within a slab with homogeneous rain.

As the frequency becomes higher, the specific attenuation associated to a rain event is progressively more dependent on the Drop Size Distributions (DSD) as a higher number of drops cause Mie scattering instead of Rayleigh scattering [3]. DSD analytical models can be found in the literature [3]-[4].

Manuscript received XXXX, XX, 2020. This work was supported in part by the Ministry of Science, Innovation and Universities of Spain through the RTI2018-098189-B-I00 project.

J.M. Riera, correspondence author, A. Benarroch, P. Garcia-del-Pino and S. Pérez-Peña are with Information Processing and Telecommunications Center, Universidad Politécnica de Madrid, ETSI de Telecomunicación, 28040 Madrid, Spain (e-mail: jm.riera@upm.es, ana@grc.ssr.upm.es, pedro.gdelpino@upm.es, santiago.ppena@gmail.com).

In this context, the use of DSD measured with different types of instruments is of relevance, especially for propagation experimental campaigns. This paper deals with the data pre-processing and calibration procedures that can be recommended for the use of experimental DSD, exploiting the large periods of DSD measured with two instruments at Escuela Técnica Superior de Ingenieros de Telecomunicación (ETSIT) of Universidad Politécnica de Madrid (UPM), Spain. The experimental DSD can be used in the prediction of the attenuation in millimeter-wave links, and the predictions can be later compared to measurements. The assessment of the quality and features of the DSD is a previous step in the general aim of using this kind of data in the context of propagation experiments.

For this study, DSD have been collected for eleven years (2007-2017) using a vertically pointing Doppler radar, the Micro Rain Radar (MRR-2) manufactured by Metek, and for ten years (2008-2017) using the optical Thies Laser disdrometer. Only liquid precipitation is considered. Snow and hail are removed. The main characteristics of these two instruments are described in Section II. Preliminary results derived from the information gathered with these instruments have been presented at conferences [5]-[6]. In both cases, pre-processing procedures are proposed in order to obtain experimental DSD with adequate quality for the application.

In order to assess the DSD dependence on the type of rain event (stratiform or convective), this paper proposes an event classification procedure that makes use of the measurements taken with the MRR-2. The procedure is based on a bright band (BB) detection method, as described in Section III, where an original calibration technique is also included for the MRR-2 data. Another event classification procedure using polarimetric radar can be found in [7] and a different BB detection strategy using a neural network approach in [8]. Section IV introduces the Laser disdrometer data processing. This instrument provides spectra of drop diameter sizes vs. terminal fall speed. The spectra must be analyzed and filtered before calculating the DSD. Several filter options have been analyzed. The Laser disdrometer measurements can be further improved through the comparison with 2D video disdrometer [9] when it is available. Section V presents the statistical results on the DSD obtained by MRR-2 and Laser disdrometer for the different types of events collected at ETSIT-UPM. Finally, Section VI draws conclusions from the study.

II. Meteorological Equipment

DSD are quantified by $N(D)$ ($\mathrm{m^{-3}mm^{-1}}$), which is the number of particles per volume ($\mathrm{m^3}$) and per diameter (mm) units. The DSD obtained by the MRR-2 and the Laser disdrometer are available in discrete bins, organized in diameter classes, D_i.

The MRR-2 is a K-band continuous wave and frequency-modulated Doppler rain radar, operating at a frequency close to 24 GHz. It is vertically pointed and provides DSD with 47 drop diameter classes, which are obtained from the backscattering of the radar signal received from 31 altitude levels. A level spacing of 100 m has been used in this case, but it can be configured for smaller or larger separations. The manufacturer provides detailed documentation [10] explaining its physical basis of operation and the data processing carried out to deliver the DSD. The DSD delivered by the instrument, using its internal software, have been used in this work, but some modifications have been applied as a result of the procedure developed for measurement calibrations.

The Thies Laser disdrometer [11] is based on an optical laser beam source that produces a parallel beam of infrared light (780 nm). At the receiver, a photo diode measures the optical intensity and converts it into an electrical signal. If a precipitation particle falls across the light beam, a reduction in the received signal will appear. Hence, it is possible to calculate the diameter and speed of the particle from the amplitude and duration of this reduction.

For the Laser disdrometer, the precipitation particles are collected every minute and are organized in a diameter-speed grid. Each bin of the grid is related to a specific combination of diameter (D_i) and speed (v_j) classes, which are classified in 22 (i = 1,…,22) and 20 (j = 1,…,20) non-uniform classes, between 0.125-8 mm and 0-10 m/s, respectively. An example of Laser disdrometer spectrum appears in Fig. 1, where the color of each bin denotes the number of particles detected during that minute. Moreover, Fig. 1 shows the Gunn-Kinzer (GK) curve [12], which models $v(D)$ (m/s), as a function of D (mm). In accordance with [13] the GK curve is adjusted considering Madrid altitude h through the term $\delta_v(h)$ (h = 680 m, then $\delta_v(h)$ = 1.025). The GK curve and its correction are described in (1)-(2). Equation (1) is strictly valid only for $0.109 \le D \le 6$ mm.

$$v(D) = (9.65 - 10.3 \cdot \exp(-0.6 \cdot D[\mathrm{mm}])) \cdot \delta_v(h) \tag{1}$$

$$\delta_v(h) = 1 + 3.68 \cdot 10^{-5} \cdot h[\mathrm{m}] + 1.71 \cdot 10^{-9} \cdot h[\mathrm{m}]^2 \tag{2}$$

DSD are calculated from the Laser disdrometer spectra with (3), where $n(D_i,v_j)$ is the number of particles with diameter class D_i (mm) and speed class v_j (m/s), S = 45.6 $\mathrm{cm^2}$ is the surface onto which the Laser disdrometer calculates the number of particles, Δt = 60 s is the integration time and dD_i (mm) is the D_i class width.

$$N(D_i) = \sum_{j=1}^{20} \frac{n(D_i,v_j)}{v_j} \cdot \frac{1}{S \cdot \Delta t \cdot dD_i} \tag{3}$$

However, before applying (3) the Laser disdrometer data must be checked and validated as it is discussed in Section IV.

Further, for both instruments, R can be calculated by integrating the contribution of all the drops (4) [10].

$$R = \frac{\pi}{6} \cdot \sum_i D_i^3 \cdot N(D_i) \cdot v(D_i) \cdot dD_i \tag{4}$$

A rain-gauge is used to calibrate the radar measurements, as will be seen further on. A tipping-bucket rain-gauge was used until 2017, when it was replaced by a weighing rain-gauge.

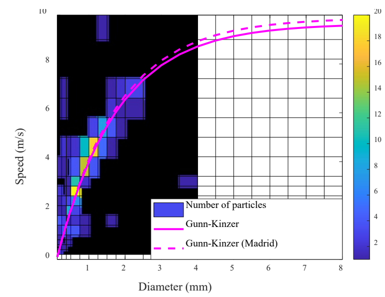

Fig. 1. An example of Thies Laser Distrometer spectrum.

The measurement principles of the two instruments are totally different. The Laser disdrometer measures individually each of the raindrops that crosses the beam surface of 45.6 $\mathrm{cm^2}$ of the instrument, whereas the MRR-2 measurements are based on the backscattering of the K-band signal in a large volume of space above the site. The main advantage of the MRR-2 is that it provides measurements at different heights. The Laser disdrometer only delivers the DSD at surface level, but is expected to be more accurate, although some filtering and processing must be applied to correct some problems that can occur in the raindrop detection.

III. Data Processing, Calibration and Event Classification Using MRR-2

The MRR-2 provides measurements every minute from 31 different heights (100−3100 meters in the configuration used in this work). The main output is the DSD for each height level; additional parameters are calculated from the DSD: R (4), Liquid Water Content (LWC), Characteristic Fall Velocity (W) and radar reflectivity (Z). The lowest possible level would be of interest to compare with the Laser disdrometer and other instruments that measure the rain at surface level. However, the first level (100 m) is usually affected by clutter from the surface; therefore, the second level is used in this work (200 m) instead.

A. DSD Calculation

The MRR-2 does not measure directly the DSD, but the Doppler power-spectra scattered by hydrometeors. The measurements are ranked by their Doppler shift. The spectral power retrieved by the radar in engineering units is [10]:

$$f(n,k) = \frac{10^{20} \cdot \mathrm{TF}(k)}{C} \cdot \frac{1}{k^2 \cdot \Delta h} \cdot \eta(n,k) \tag{5}$$

where n is the number of the Doppler spectrum line (n = 0, ..., 63), k is the gate height number (k = 1, ..., 31), TF (k) is the transfer function, C is an internal calibration constant, Δh (m) is the height resolution and $\eta(n,k)$ ($\mathrm{m^{-1}}$) is the spectral reflectivity, or backscatter section by volume. Both TF (k) and C are stored in the radar firmware.

The distributions of drop speeds can be derived from the Doppler spectra gathered by the radar. To obtain the DSD, the modified GK relationship described in (1)-(2) is used. This relationship is defined for liquid drops; hence, the DSD and parameters derived from them are only valid for liquid precipitation. The raw spectral power distribution (5) is calculated for equally spaced Doppler classes, which are straightforwardly associated to equally spaced speed classes. When (1)-(2) are applied, the resulting drop size classes are not equally spaced. Moreover, they change with height, because of the correction (2) taken from [13]. The maximum diameters measured with this instrument are about 5 mm, the exact value dependent on the height level.

The spectral reflectivity density with respect to the drop diameter, $\eta(D,k)$, can be obtained from the spectral reflectivity density with respect to speed, $\eta(v,k)$, as follows [10]:

$$\eta(D,k) = \eta(v,k) \cdot 6.18 \exp(-0.6 \cdot D[\mathrm{mm}]) \cdot \delta_v(k \cdot \Delta h) \qquad (6)$$

where $\eta(v,k) = \eta(n,k)/\Delta v$, Δv being the speed resolution calculated from the frequency resolution of the Doppler spectra $\Delta f = 30.52$ Hz, which gives $\Delta v = \Delta f \cdot \lambda/2 = 0.1887$ ms^{-1}.

The number of particles per volume and diameter units, $N(D,k)$, is the quotient between $\eta(D,k)$ and the raindrop backscattering cross section $\sigma(D)$ of drops with diameter D.

Since not all drop diameters are small with respect to the signal wavelength λ, the Rayleigh approximation cannot be applied and Mie scattering in spherical and homogeneous particles is used instead to calculate $\sigma(D)$ [3].

All other parameters obtained from the radar measurements are calculated from v, η and the DSD [14]. Regarding wind effects, stagnant air is assumed in (1). The analysis of errors due to vertical wind performed in [10] has found no improvement when a vertical wind correction is applied.

B. Events Identification and Calibration

It has been found that the MRR-2 may underestimate or overestimate the values of R, by an amount that depends on the type of rain event [15]. This fact has been confirmed in this study and has led to develop a new calibration procedure.

The MRR-2 offers an internal calibration method which is not effective in our case in correcting this mismatch because of the insufficient stability of the calibration constant for different events, even on the same day. This mismatch is solved by calculating an adjustment factor (C_F) for each individual rain event, which is obtained by comparing the average R of the MRR-2 for the event and the one calculated from the data measured by the rain-gauge and the Laser disdrometer. For calibration, the time series of R obtained by the rain-gauge were preferably used, they were replaced with the R collected by the Laser disdrometer when the rain-gauge was malfunctioning. C_F is directly applied on most of the parameters collected by the MRR-2 including the DSD, that are multiplied by its value, since R is proportional to $N(D_i)$ as shown in (4) and C_F is expected to be the same for all D_i.

Rain events are identified and separated by using the time series of R of the different instruments. A rain event is considered to end when it is followed by at least 20 consecutive minutes without registered R.

C. Analysis and Classification of Events

In temperate climates, it is possible to classify rain events as convective or stratiform. Convective events are related to small cell extension and high R, and stratiform events are associated to larger horizontal extension, and lower R. Event classification is useful in several meteorological applications, particularly for understanding the physics of clouds, since the two types of rain events are connected to different cloud growth mechanisms. Furthermore, rain attenuation estimations can benefit from an accurate event classification [16].

As soon as the rain events have been separated and calibrated, they are processed for classifying them as stratiform or convective. The main rain event indicators useful for the assessment of the classification are: the maximum R (R_{max}), a parameter obtained directly from the MRR-2 data, and the percentage of BB appearance during the rain event, the latter being obtained with the procedure explained below.

D. Bright Band Detection

The BB is a layer with higher radar reflectivity, typically a few hundred meters thick. The BB arises due to the difference between the water and ice dielectric constant, and due to the aggregation of ice particles into snowflakes as they descend and melt. Above the BB there are ice crystals with large diameter, but with small dielectric constant, meaning that their reflectivity is low. Beneath the BB, liquid particles with larger dielectric constant arise but they have a reduced diameter.

During the transition from solid to liquid, the snowflakes begin to melt; at that time, a liquid layer covers them just before the particles melt and break up into others with reduced diameter. This is why the BB is also known as the melting layer. Such large particles formed by ice crystal cores with liquid coverage, with a high dielectric constant, produce the BB in radar measurements due to their high reflectivity [17].

Aside from a reflectivity increment, the BB is associated with a higher Differential Vertical Velocity (DVV) [17] since the fall speed generally increases as the snowflakes (<2 ms^{-1}) fuse in large rain particles (>5 ms^{-1}). This is the basis of the procedure employed in this study for the estimation of the BB appearance. Starting from the DVV, the procedure involves a five-coefficient Finite Impulse Response (FIR) filter, a median filter to minimize noise, a detector of peaks exceeding a minimum threshold, an evaluation of the layers close to the peaks with maximum DVV and an averaging of the results.

Fig. 2 shows an example of the estimator. It corresponds to a typical stratiform event registered on April 2nd, 2014. Fig. 2 consists of: a) the reference time series of R, that is obtained from the rain-gauge or the Laser disdrometer depending on the event, and the time series of R derived from the calibrated MRR-2 data; b) 2D maps of reflectivity, fall speed and filtered DVV vs time and height above surface level. From the latter, the BB height is easily estimated for this event. The procedure delivers the height above surface of the BB bottom part (approx. 1150 m in this case), its depth being typically 300-400 m, with the radar resolution of 100 m.

A typical convective event, registered on October 4th, 2013, is shown in Fig. 3. The expected differences between stratiform and convective events are clearly appreciated in the comparison of Fig. 2 and 3. In Fig. 2 the precipitation structure is noticeably seen as stratified, with a defined transition between liquid and solid precipitation, in the plots of reflectivity and fall speed, whereas in Fig. 3 the lack of an equivalent transition are apparent. The BB altitude is clearly identified for most of the event duration in Fig. 2, whereas its detection is not possible in Fig. 3.

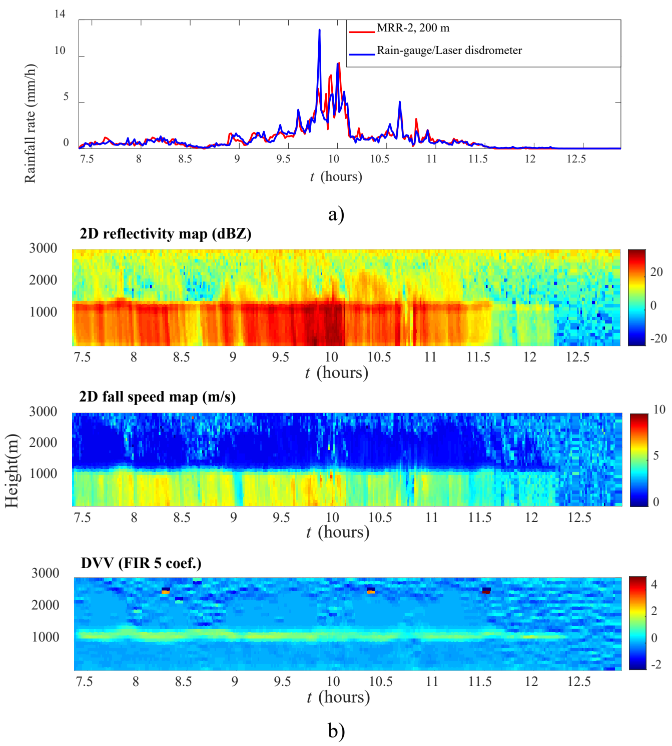

Fig. 2. Stratiform event registered on April 2, 2014. a) Time series of rain-gauge/Laser disdrometer and calibrated MRR-2 R. b) (Top) 2D reflectivity map (dBZ), (middle) 2D fall speed map (m/s), (bottom) DVV (FIR 5 coef.).

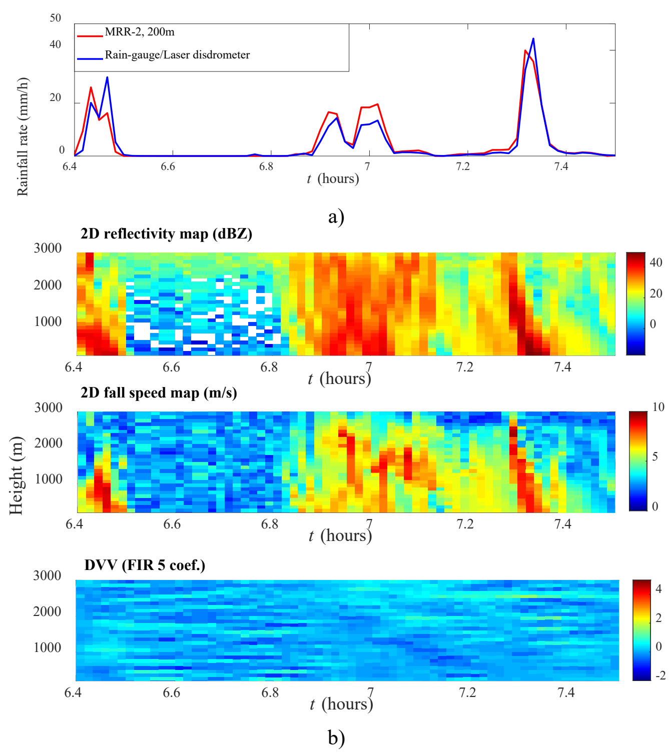

Fig. 3. Convective event registered on October 4, 2013. a) Time series of rain-gauge/Laser disdrometer and calibrated MRR-2 R. b) (Top) 2D reflectivity map (dBZ), (middle) 2D fall speed map (m/s), (bottom) DVV (FIR 5 coef.).

As a result of detailed analysis of the data registered in this period, the events were classified according to the following criteria: events with R_{max} < 5 mm/h were considered as stratiform and events with $R_{max} \geq 14$ mm/h as convective. The events with values between 5 mm/h and 14 mm/h were classified as stratiform if the BB is detected for equal or more than 30% of the event duration and convective if BB presence is less than 30% of the event duration.

IV. Thies Laser Disdrometer Data Pre-Processing

Before calculating the DSD using (3) Laser disdrometer data must be pre-processed in order to discard instrument errors, maintain data integrity and select only the particles drawn from liquid rain measurements. DSD are obtained for the D_i used by the instrument, with dD_i of 0.125 mm ($D_i < 0.5$ mm), 0.25 mm ($0.5 \leq D_i < 2$ mm) and 0.5 mm ($D_i \geq 2$ mm).

The comparison with reference rain-gauges in [18] reveals that the Thies Laser disdrometer generally measures larger R amounts than the reference rain-gauges, also it tends to overrate R during strong convective events. There are various reasons for these errors, for example, the Laser disdrometer may detect as a single large drop a group of multiple simultaneous drops [19]; it could also be possible that particles hitting the rim of the light beam are interpreted as too small particles. Hence, in [20], the bias between Laser disdrometers and other rain-gauges was related, not only to the uncertainty in the evaluation of the diameter or to wind effects, but also to inaccuracies in the determination of the sensing area.

Hence, a first data quality control and several particle filters were evaluated in a previous work of our group [6], which was incorporated in [21]. In this paper, we compared two different particles filters, Filters A and B, combined with the previous data quality control and initial filtering procedure.

The initial data quality control is used to detect drizzle and noise in an individual one-minute rain event spectrum. A spectrum is deemed as noise and is removed if it has less than 10 particles with an $R < 0.1$ mm/h [22]. And it is considered as drizzle if at least 95% of the particles in the spectrum have a $D \leq 0.5$ mm and more than 99% have a $D \leq 1$ mm.

An initial filtering procedure is applied over particles with relatively large diameters and low speeds, because they can be spurious particles or snowflakes. It is performed following the Locatelli-Hobbs empirical diameter–fall speed relationship [23]. Besides, isolated particles located at a given distance from the main cluster of bins containing particles are also removed. A distance between 2 and 4 empty bins has been used in [24] (distance 4 has been selected for this paper).

Filter A: for particles with speeds 60% above or below the modified GK curve. They are considered as erroneous (due to splashing, wind or particles falling through the edges of the sensing area). This procedure was proposed in [25].

For a minute classified as drizzle, Filter A was not applied, since a drizzle spectrum normally contains clusters of particles that do not fit the reference of the GK curve (because the particles are concentrated in the smallest diameters).

Filter B: for very small particles, up to 1 mm, with very high fall speeds. To do so, a speed threshold should be chosen as a compromise between fall speeds of real and spurious particles [26]-[27]. Pursuing this, fall speed histograms derived for the smaller diameter bins for one stratiform event and for one convective event reveal that for more than 6 m/s the frequency of appearance of small drops is less than 2.5 % [21]. Hence, a threshold of 6.6 m/s has been established, so that particles of $D < 1$ mm are removed if they pass this speed.

It must be noted that individual particles were removed but not the full one-minute spectrum that contains such particles.

The impact of particle filters on the Laser disdrometer DSD (3) calculated for 2017 has been investigated for different R intervals. Fig. 4 presents the average DSD for R in the interval $10 < R \leq 20$ mm/h calculated from the unfiltered and filtered spectra by Filter A and B, both filters include the initial filtering procedure described above. The main effect of the filters is apparent on the larger diameter particles. Notice that the R intervals are established using the integrated R calculated from (4) with the filtered DSD.

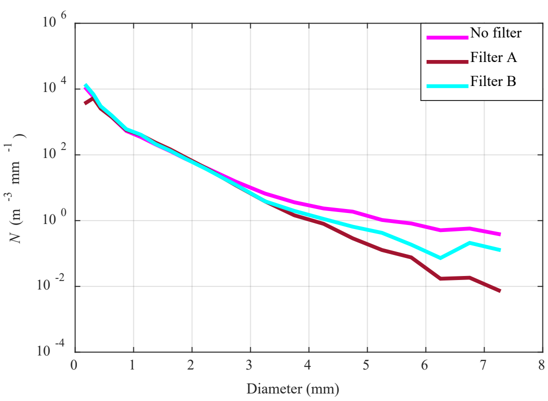

Fig. 4. Effect of Filter A and B on the average DSD calculated from the Laser disdrometer data for 2017, for very heavy R ($10<R\leq20$mm/h).

Fig. 5 shows the integrated R distributions obtained from (4) collected in 2017 without and after applying filters. The solid blue line is the distribution of the R provided by the Laser disdrometer, as calculated by the instrument software. With the application of Filter B, the R are very close to the R calculated by the instrument.

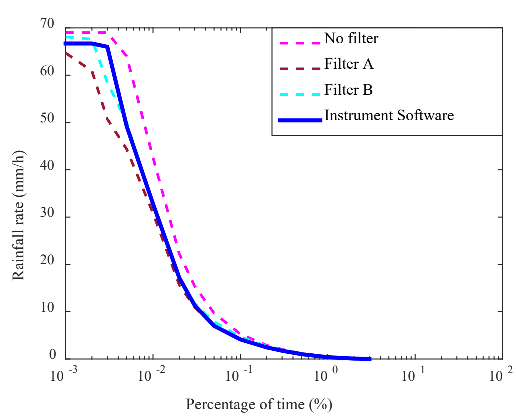

Fig. 5. Filter A and B effect on the Complementary Cumulative Distribution function (CCFD) of R calculated from the Laser disdrometer data for 2017.

It is recognizable that the Laser disdrometer software applies some filtering before calculating the R, although this information is not provided in the available literature [11]. In Fig. 5 Filter A yielded a significant reduction in the frequency of appearance of the highest R.

It was found that Filter A removed an excessive number of particles, causing unrealistic effects both in the DSD and the distributions of R [6], [21]. Considering the above analysis, it was concluded that the best option seems to be Filter B.

V. DSD Statistics from MRR-2 and Laser Disdrometer

The DSD given by the calibrated MRR-2 at 200 m and by the Laser disdrometer, the latter after particle filtering using Filter B, have been categorized within six intervals in accordance with their integrated R (4): very light ($0<R\leq1$ mm/h), light ($1<R\leq2$ mm/h), moderate ($2<R\leq5$ mm/h), heavy ($5<R\leq10$ mm/h), very heavy ($10<R\leq20$ mm/h) and extreme ($R>20$ mm/h). Finally, yearly and average-year mean DSD have been obtained.

The average DSD measured by the MRR-2 for the light rain interval is shown in Fig. 6. Fig. 7 shows the average DSD obtained by the Laser disdrometer for the same R interval. Fig. 8-9 show, respectively, the average DSD collected by the radar and Laser disdrometer for the very heavy rain interval.

As seen in Fig. 6-7 and Fig 8-9, in the range of R values where both instruments provide measurements, both yield very similar DSD on average, except for the smallest diameters, where the number of drops obtained by the MRR-2 is significantly higher than that provided by the Laser disdrometer. This effect is more prominent for the higher rain rates, as seen in the comparison of Fig. 8-9, and is probably unrealistic, although this should be confirmed in the future by comparisons with other instruments providing reliable values of DSD for very small diameters (< 0.5 mm). For the larger diameters, both instruments provide similar results for the lower rain rates of Fig. 6-7. DSD corresponding to higher rain rates include significant numbers of drops with diameters in excess of 5 mm, as seen in Fig. 9. These large drops are not included in the DSD delivered by the MRR-2.

It must be pointed out that, although the Laser disdrometer measures particles with larger diameters, the MRR-2 provides finer resolution for small and intermediate diameters: 47 classes of diameters compared to 22 for the Laser disdrometer.

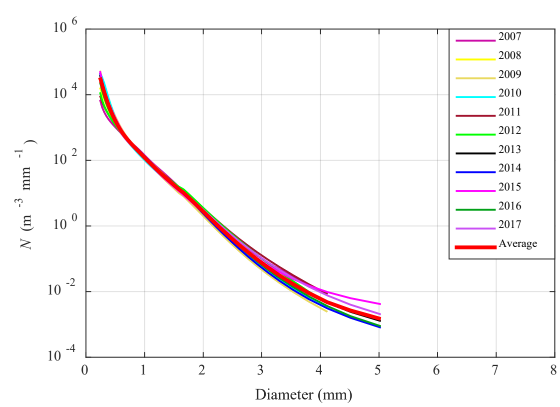

Fig. 6. Yearly and average-year distributions for light R ($1<R\leq2$ mm/h), MRR-2 radar.

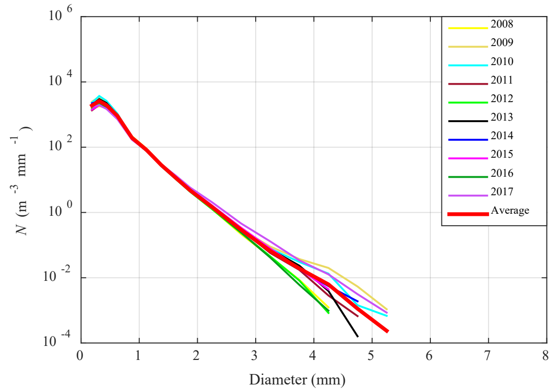

Fig. 7. Yearly and average-year distributions for light R ($1<R\leq2$ mm/h), Thies Laser disdrometer.

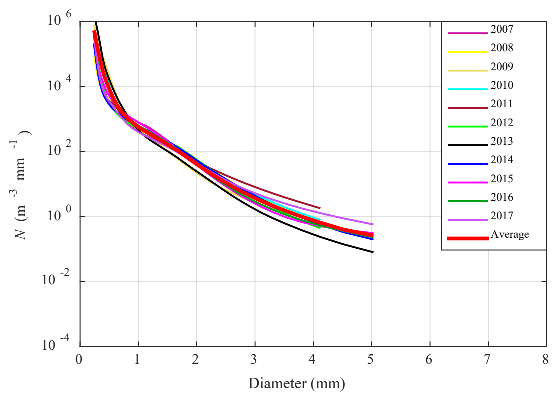

Fig. 8. Yearly and average-year distributions for very heavy R ($10<R\leq20$ mm/h), MRR-2 radar.

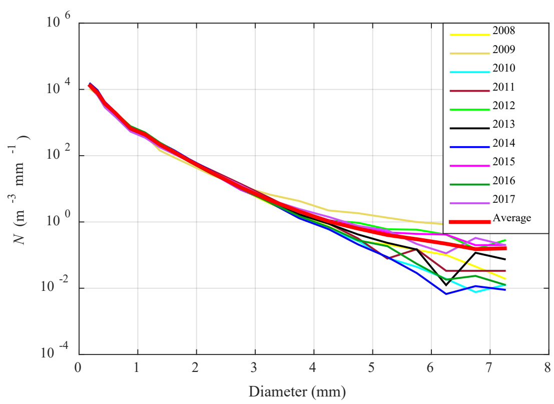

Fig. 9. Yearly and average-year distributions for very heavy R ($10<R\leq20$ mm/h), Thies Laser disdrometer.

For all R interval, average DSD have been calculated for each of the eleven (2007-2017) and ten (2008-2017) years of measurements of the MRR-2 and Laser disdrometer, respectively, according to the event types, convective or stratiform. Once the type of an event registered by the MRR-2 has been determined following the procedure described in section III, the same type is assigned to the same event measured by the Laser disdrometer. The results are in Fig. 10 for the MRR-2 and Fig. 11 for the Laser disdrometer. Both instruments collected a higher number of larger drops in the case of higher R, so that the distributions become flatter as the R increases. This flattening effect is observed for both stratiform and convective events.

As a reference, the Marshall-Palmer (M-P) distributions [28] calculated for each rain rate interval have also been included in Fig. 10-11. In this classical work an exponential law is proposed for the DSD:

$$N(D) = N_0 e^{-\Lambda D} \tag{7}$$

with $N_0 = 8000$ m^{-3}mm^{-1} and $\Lambda = 4.1\,R^{-0.21}$ mm^{-1}. The central value of R of each rain rate interval has been used in the M-P distributions, except for the highest interval, for which a reference value of $R = 30$ mm/h has been used.

The agreement between the M-P curves and the experimental DSD is better for the Laser disdrometer measurements, with relevant differences only for the largest diameters. In the case of the MRR-2 significant differences appear also in the lowest-diameter range.

As was explained in Section IV, drops crossing simultaneously the laser beam may be detected as a single one with larger diameter [19]. That would explain the higher number of drops registered by the Laser disdrometer in the largest classes, for the highest R (above 10 mm/h). For the lowest R, the radar measures a larger number of drops of large diameters. Since the MRR-2 makes use of the GK curve to derive raindrop diameters, drops are allocated along this curve according to their velocity, so that small drops that present high speeds are wrongly classified as having large diameters.

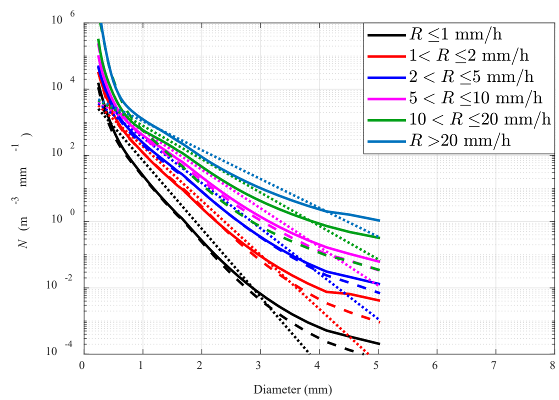

Fig. 10. Average-year distributions for each R interval, MRR-2 radar. Stratiform events (dashed), convective events (solid) and M-P (dotted).

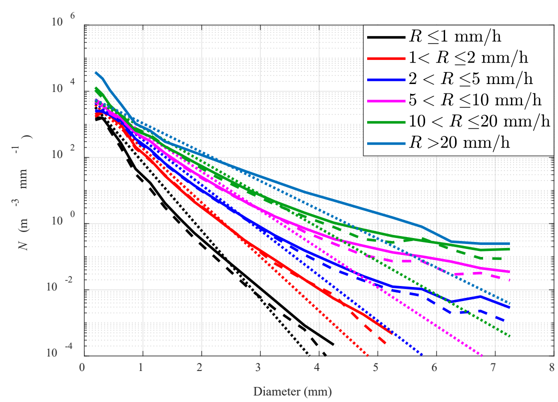

Fig. 11. Average-year distributions for each R interval, Thies Laser disdrometer. Stratiform events (dashed), convective events (solid) and M-P (dotted).

VI. Conclusions

In this research, a large database with more than ten years of DSD collected with two different instruments (a vertically-pointed K-band MRR-2 radar and a Thies Laser disdrometer) has been used to characterize the differences between the measurements of both instruments and their respective needs in terms of calibration and data pre-processing.

The measurements obtained by the MRR-2 confirm the necessity of applying the calibration procedure that has been satisfactory implemented. A method to identify and separate stratiform and convective events is proposed, based on the peak rainfall rate of the event and the BB detection method developed within this work. Event classification is important for propagation experiments.

For the Laser disdrometer, a procedure of particle filtering is necessary, which, as detailed in this work, tries to eliminate all the non-valid particles, caused by inaccuracies in the equipment, and non-liquid particles. As a result, an appropriate filtering procedure has been proposed in the paper.

Once the calibration is applied to the MRR-2 DSD and the proposed filter is used over the Laser disdrometer spectra, the two instruments have been found to provide very similar average DSD for different R ranges, for both stratiform and convective events. The differences can be explained by the different features of the two instruments.

For future works, the focus will be on obtaining rain attenuation time series derived from the experimental DSD, depending on stratiform and convective events, and comparing them with attenuation measurements available for horizontal radio links.

Acknowledgments

The authors would like to express their recognition to Dr. Jose García-Rubia and to the Master students Nicolás Gil-de-Vergara and Marta Munilla-Diez for their participation in some phases of this research activity.

References

[1] ITU-R Rec. P.838-3, “Specific attenuation model for rain for use in prediction methods,” ITU, Geneva, Switzerland, 2005.

[2] R. L. Olsen, D. V. Rogers and D. B. Hodge, "The aRb relation in the calculation of rain attenuation," *IEEE Trans. Antennas Propag.*, vol. 26, no. 2, pp. 318-329, Mar. 1978.

[3] G. Brussaard and P. A. Watson, "Physical properties of hydrometeors" in *Atmospheric modelling and millimetre wave propagation*, London, UK: Chapman & Hall, 1995, pp. 329.

[4] C. W. Ulbrich, "Natural variations in the analytical form of the raindrop size distribution", *J. Appl. Meteorol.,* vol. 22, no. 10, pp. 1764–1775, Oct. 1983.

[5] N. Gil-de-Vergara, J.M. Riera, S. Pérez-Peña, J. García-Rubia and A. Benarroch, “Classification of rainfall events and evaluation of Drop Size Distributions using a K-band doppler radar,” in *Proc. 12th Eur. Conf. Antennas Propag.*, London, UK, Apr. 9-13, 2018.

[6] S. Pérez-Peña, J. M. Riera, A. Benarroch, M. Munilla-Diez and J. García-Rubia, “Assessment of Drop Size Distributions obtained by different instruments and their application to W-band propagation studies,” in *Proc. 13th Eur. Conf. Antennas Propag.*, Krakow, PL, Mar. 31-Apr. 5, 2019.

[7] Y. Wang, L. Tang, P.-L. Chang and Y.-S. Tang, “Separation of Convective and Stratiform Precipitation Using Polarimetric Radar Data with A Support Vector Machine Method,” *Atmos. Meas. Tech.*, Discuss. Dec. 2019.

[8] M. Brast and P. Markmann, “Detecting the Melting Layer with a Micro Rain Radar Using a Neural Network Approach,” *Atmos. Meas. Tech.*, Discuss. Sep. 2019.

[9] M. Fehlmann, M. Rohrer, A. von Lerber and M. Stoffel, “Automated precipitation monitoring with the Thies disdrometer: Biases and ways for improvement,” *Atmos. Meas. Tech.*, Discuss. Jan. 2020.

[10] METEK, “MRR Physical Basics,” 2010.

[11] ADOLF THIES GmbH & Co. KG, “Laser Precipitation Monitor, Instruction for Use,” v2.0x STD, 2005.

[12] R. Gunn and G. D. Kinzer, “The terminal velocity of fall for water droplets in stagnant air,” *J. Meteor.,* vol.6, no.4, pp. 243-248, Aug. 1949.

[13] G. B. Foote and P. S. Du Toit, “Terminal velocity of raindrops aloft," *J. Appl. Meteorol.*, vol. 8, no. 2, pp. 249-253, Apr. 1969.

[14] METEK, “Micro Rain Radar User Manual,” March 2012.

[15] O. P. Prat and A. P. Barros, “Ground observations to characterize the spatial gradients and vertical structure of orographic precipitation – Experiments in the inner region of the Great Smoky Mountains,” *J. Hydrol.*, vol. 391, no. 1, pp. 141-156, Sept. 2010.

[16] E. N. Anagnostou, “A convective/stratiform precipitation classification algorithm for volume scanning weather radar observations,” *J. Meteorol. Appl.*, vol. 11, no. 4, pp. 291-300, Dec. 2006.

[17] A. B. White, D. J Gottas, E. T. Strem, F. M. Ralph and P. J. Neiman, “An Automated Brightband Height Detection Algorithm for Use with Doppler Radar Spectral Moments,” *J. Atmos. Ocean. Tech.*, vol. 19, no.5, pp.687-697, May 2002.

[18] E. Vuerich, C. Monesi, L. G. Lanza, L. Stagi and E. Lanzinger, “ The WMO field intercomparison of rain intensity gauges,” *Atmos Res*, vol. 94, issue 4, pp. 534–543, Jan. 2009.

[19] E. Lanzinger, M. Theel and H. Windolph, “Rainfall amount and intensity measured by the Thies laser precipitation monitor,” TECO-2006, Geneva, Switzerland.

[20] R. P. d. M. Frasson, L. K. da Cunha and W. F. Krajewski, “Assessment of the Thies optical disdrometer performance,” *Atmos Res*, vol. 101, no. 1-2, pp. 237-255, July 2011.

[21] ITU-R Doc. 3J/FAS/7 - Fascicle on the processing of drop size distribution and data for Study Group 3 Experimental Database, Rev.2, May 2019, ITU, Geneva Switzerland.

[22] A. Tokay, W. A. Petersen, P. Gatlin and M. Wingo, “Comparison of raindrop size distribution measurements by collocated disdrometers,” *J. Atmos. Ocean. Tech.*, vol. 30, no. 8, pp. 1672–1690, Aug. 2013.

[23] J. D. Locatelli and P. V. Hobbs, “Fall speeds and masses of solid precipitation particles,” *J. Geophys. Res.*, vol. 79, no. 15, pp. 2185–2197, May 1974.

[24] J. M. Garcia-Rubia, J. M. Riera, A. Benarroch, and P. Garcia-del-Pino, "Estimation of rain attenuation from experimental Drop Size Distributions," *IEEE Antennas Wireless Propag. Lett.*, vol. 10, pp. 839-842, Aug. 2011.

[25] K. Friedrich, S. Higgins, F. J. Masters and C. R. Lopez, “Articulating and stationary PARSIVEL disdrometer measurements in conditions with strong winds and heavy rainfall,” *J. Atmos. Ocean. Tech.*, vol. 30, no. 9, pp. 2063–2080, Sept. 2013.

[26] M. Thurai *et al.,* “Toward completing the raindrops size spectrum: case studies involving 2-D-video disdrometer, droplet spectrometer, and polarimetric radar measurements,” *J. Appl. Meteorol. Clim.*, vol. 56, no. 4, pp. 877–896, Apr. 2017.

[27] V. N. Bringi, M. Thurai and D. Baumgardner, “Raindrop fall velocities from an optical array probe and 2-D video disdrometer,” *Atmos. Meas. Tech.*, vol. 11, no. 3, pp. 1377-1384, Mar. 2018.

[28] J. S. Marshall and W. M. K. Palmer, "The distribution of raindrops with size", *J. Meteorol.,* vol. 5, pp. 165-166, 1948.